Cell wall peptidoglycan architecture in *Bacillus subtilis*

Emma J. Hayhurst*, Lekshmi Kailas[†‡], Jamie K. Hobbs[†‡], and Simon J. Foster*[§]

*Department of Molecular Biology and Biotechnology, University of Sheffield, Firth Court, Western Bank, Sheffield S10 2TN, United Kingdom; [†]Department of Chemistry, University of Sheffield, Western Bank, Sheffield, S3 7HF, United Kingdom; and [‡]Department of Physics and Astronomy, University of Sheffield, The Hicks Building, Hounsfield Road, Sheffield, S3 7RH, United Kingdom

Edited by Thomas J. Silhavy, Princeton University, Princeton, NJ, and approved July 15, 2008 (received for review April 29, 2008)

The bacterial cell wall is essential for viability and shape determination. Cell wall structural dynamics allowing growth and division, while maintaining integrity is a basic problem governing the life of bacteria. The polymer peptidoglycan is the main structural component for most bacteria and is made up of glycan strands that are cross-linked by peptide side chains. Despite study and speculation over many years, peptidoglycan architecture has remained largely elusive. Here, we show that the model rod-shaped bacterium *Bacillus subtilis* has glycan strands up to 5 μm, longer than the cell itself and 50 times longer than previously proposed. Atomic force microscopy revealed the glycan strands to be part of a peptidoglycan architecture allowing cell growth and division. The inner surface of the cell wall has a regular macrostructure with $\approx$50 nm-wide peptidoglycan cables [average 53 $\pm$ 12 nm (n = 91)] running basically across the short axis of the cell. Cross striations with an average periodicity of 25 $\pm$ 9 nm (n = 96) along each cable are also present. The fundamental cabling architecture is also maintained during septal development as part of cell division. We propose a coiled-coil model for peptidoglycan architecture encompassing our data and recent evidence concerning the biosynthetic machinery for this essential polymer.

The major structural polymer in the cell walls of most eubacteria is peptidoglycan, which is responsible for shape determination and cellular viability. It is a complex polymer made up of glycan strands of repeating disaccharide residues, cross-linked via peptide side chains (1). It has a dynamic structure, continuously being synthesized, modified, and hydrolyzed to allow for cell growth and division, among many other roles (2). The peptidoglycan is essential to allow a high internal osmotic pressure inside the cell to be maintained. The crucial importance of this polymer is exemplified by the range of antibiotics that specifically target its synthesis. These include the β-lactams and glycopeptides, which have had such a positive impact on human health. Much is now known about the roles of multiple biosynthetic, modification, and autolysis enzymes in peptidoglycan dynamics (2), and biochemical studies have revealed that these systems result in a complex, mature peptidoglycan structure (3, 4). Biochemical analysis generally requires hydrolysis with a muramidase, resulting in release of muropeptide fragments. However, any information as to the length of the glycan strands is lost. An HPLC separation technique has been developed to specifically address the issue of glycan strand length (5). This has only been applied to two organisms, and both were found to have surprisingly short strands. In *Escherichia coli*, strands have an average length of 21 disaccharide residues (5), and in *Staphylococcus aureus*, they are even shorter at an average of 6 disaccharides, much less than proposed (6, 7).

The classic model for peptidoglycan architecture suggests that the glycan strands run parallel to the plasma membrane (8), arranged perhaps as hoops or helices around the short axis of the cell resulting in a woven fabric (9). However, the discovery of very short glycan strands has led to the proposal of a "scaffold" model in which the strands are oriented vertically in respect to the membrane (10, 11), although this hypothesis is controversial (12). The application of high-resolution, atomic force microscopy (AFM) to the study of the structure of the outer surface of *S. aureus* and *Bacillus atrophaeus* cell wall peptidoglycan reveals a surface network of thin fibers (possibly of only a few glycan strands) with large empty spaces in between (13, 14). This is supported by an NMR structural analysis in which a "honeycomb" architecture, based on the scaffold model, is proposed for the peptidoglycan of *E. coli* (15).

Even though we understand a large amount about how peptidoglycan is synthesized, modified, and hydrolyzed, how this relates to its stress-bearing, dynamic structure is still largely obscure. Also, how peptidoglycan architecture allows bacteria to assume even relatively simple morphology, such as a rod, is unknown. Any architectural model must also account for the insertion of new material to permit cell growth. Random insertion of nascent peptidoglycan in rod shaped organisms is unlikely, especially because of the discovery of both helical tracking of the biosynthetic machinery and vancomycin labeling of new material in helices (16, 17). A helical model of insertion of cell wall material has been discussed (12, 17–19) but remains unproven without direct architectural evidence.

Bacillus subtilis is a rod-shaped organism about which much is known concerning structure and the function of the cell wall. The chemistry of the cell wall peptidoglycan has been well established (4), and an average glycan strand length of 96 disaccharides has been proposed (7). Here, we have investigated the glycan strand length of *B. subtilis*, finding a population of extremely long strands. Furthermore, high-resolution AFM analysis has discovered an unexpected and elegant peptidoglycan architecture. This provides a model of cell wall architecture and presents exciting opportunities to explain one of the most fundamental aspects of bacterial growth and division.

Results and Discussion

Glycan Strand Length in *B. subtilis*. To determine the strand length of the glycans in *B. subtilis*, a method was developed based on that used for *S. aureus* (6). Purified peptidoglycan labeled with *N*-acetyl [^{14}C]glucosamine was digested overnight with the *S. aureus* amidase Atl. This resulted in solubilization of 96 $\pm$ 4% (n = 5) of the radiolabeled peptidoglycan [see supporting information (SI) *Text*]. Glycan strands were separated from peptide side chains by using ion exchange chromatography and the glycan fraction verified by using radiolabeled material (see *SI Text* and Fig. S1). Peptidoglycan digestion using the Atl

Author contributions: E.J.H., J.K.H., and S.J.F. designed research; E.J.H. and L.K. performed research; E.J.H., L.K., J.K.H., and S.J.F. analyzed data; and E.J.H., J.K.H., and S.J.F. wrote the paper.

The authors declare no conflict of interest.

This article is a PNAS Direct Submission.

[§]To whom correspondence should be addressed. E-mail: S.Foster@sheffield.ac.uk.

This article contains supporting information online at www.pnas.org/cgi/content/full/0804138105/DCSupplemental.

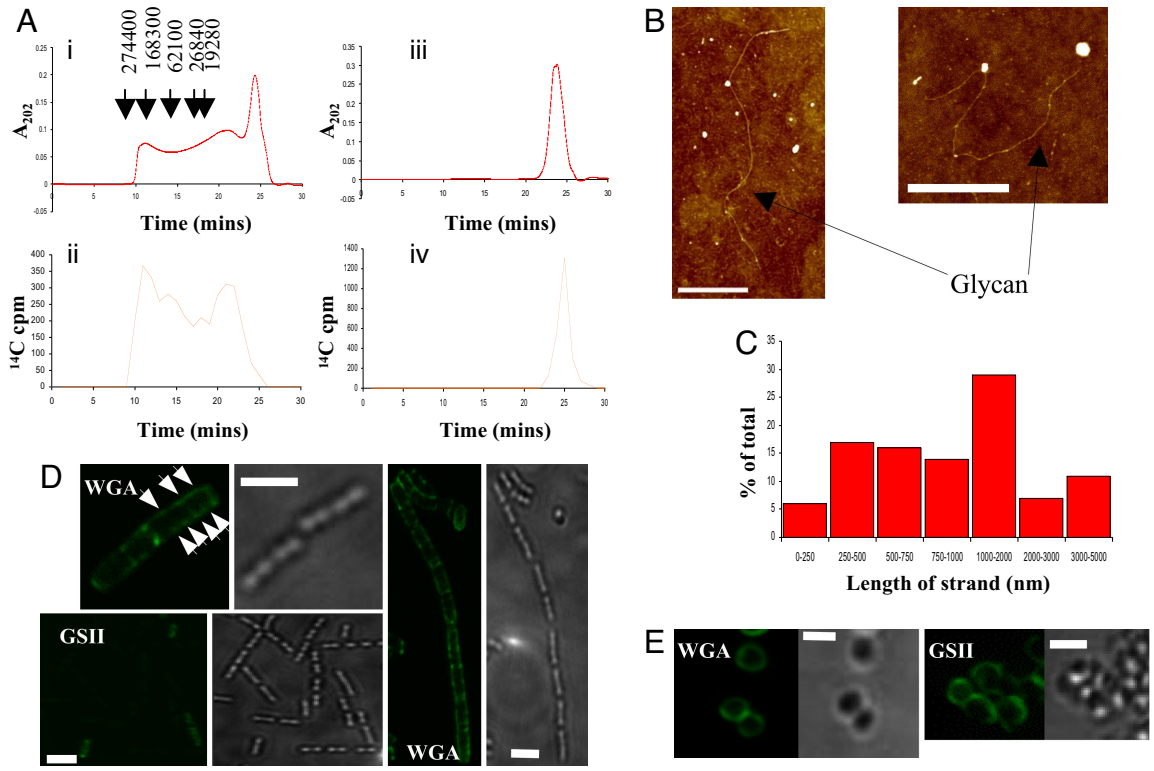

Fig. 1. *B. subtilis* glycan strand length determination. (*A*) Size exclusion chromatography of *B. subtilis* 168 HR amidase digested and ion exchange purified glycan. Glycan containing material has a large mass range (*i*) verified by *N*-acetyl [^{14}C]glucosamine labeling (*ii*). Muramidase (Cellosyl) hydrolysis confirms the material as glycan (*iii* and *iv*). In (*i*), arrows indicate the elution times of linear molecular standards of polyethylene oxide (Polymer Laboratories) of masses shown. (*B*) AFM height images of isolated glycan strands (eluted at 10–12.5 min in *A*). Z (height) range = 5 nm. (Scale bar, 1 μm.) (*C*) Length distribution of isolated *B. subtilis* glycan strands. Measured are 83 strands from AFM images. (*D*) *B. subtilis* cell wall peptidoglycan labeled with WGA or GSII. Both lectin-labeled fluorescent and corresponding bright field images are shown. Arrows indicate labeled bands and spots characteristic of a helical arrangement. (Scale bar, 2 μm) (*E*) *S. aureus* cell wall peptidoglycan labeled with WGA or GSII. Both lectin-labeled fluorescent and corresponding light field images are shown. (Scale bar, 1 μm.)

amidase, and thus, the absence of any remaining peptide cross-links, was also confirmed by using both amino acid and muropeptide analysis of the ion exchange purified material (see *SI Text* and Figs. S2 and S3). Using the established method of reverse phase chromatography on the purified glycan material (6) allowed resolution of *S. aureus* but not *B. subtilis* glycan strands (data not shown). Size exclusion chromatography of the *B. subtilis* glycan material revealed a broad mass distribution, including ≈25% of radiolabeled glycan eluting at approximately the same as the void volume of the column (Fig. 1*A*), indicating a mass of >250 kDa or 500 disaccharides. Muramidase digestion of the material into its constituent disaccharides resulted in the expected loss of the high mass peak (Fig. 1*A*). Radioactivity of the column eluate corresponded to the absorbance peaks, confirming these as glycan material.

To resolve the glycan strand length, AFM was used on size exclusion purified glycan (eluted at 10–12.5 min) (Fig. 1*A*). Surprisingly, individual glycan strands of up to 5 μm in length were found (Fig. 1*B* and Fig. S4), corresponding to 5,000 disaccharides, because one disaccharide is ≈1 nm in length (20). Measurement of 83 strands (Fig. 1*C*) from the size exclusion high mass fraction (eluted at 10–12.5 min) (Fig. 1*A*) gave an average of 1.3 μm (1,300 disaccharides). Using an identical method to that described for *B. subtilis*, glycan purified from *S. aureus* did not reveal any strand-like features when imaged by using AFM (data not shown). A Cellosyl-digested *B. subtilis* glycan sample, as well as a buffer-only sample, was also lacking strands (data not shown). Thus, *B. subtilis* has glycan strands up to 50 times longer than determined by differential sodium borohydride labeling (7), which could only show average strand length.

To visualize peptidoglycan distribution in whole cells, differential lectin-labeling and fluorescence microscopy were used (Fig. 1*D*). Cells were chemically extracted to remove accessory polymers containing GlcNAc and treated with wheat germ agglutinin (WGA), to label peptidoglycan associated GlcNAc residues (21), or *Griffonia simplicifolia* lectin II (GSII), a lectin that specifically labels nonreducing GlcNAc termini (22). Cells with shorter glycan strands would, therefore, fluoresce more when labeled with GSII compared with cells with longer strands. *S. aureus*, with an average glycan strand length of six disaccharides (6), was used as a control. Cell walls of *B. subtilis* have a much increased overall labeling with WGA compared with GSII (Fig. 1*D*), whereas in *S. aureus*, relative levels are comparable (Fig. 1*E*). The small proportion (<10%) of *B. subtilis* cells demonstrating any GSII binding is most likely because of partial lysis because <1% of cells are labeled in a *sigD* mutant (data not shown). SigD is known to control autolysis and the expression of several peptidoglycan hydrolases (23). Purified broken sacculi show the same differential lectin binding (data not shown). Interestingly, WGA does not bind the peptidoglycan of *B. subtilis* uniformly but shows cross striations reminiscent of the helical structures observed for the cytoskeletal-associated elements MreC and MreD (16) (proposed to track the peptidoglycan biosynthetic machinery) and nascent peptidoglycan labeled with fluorescent vancomycin (6). Previously, WGA labeling has not shown such detail, likely because of the presence of GlcNAc in teichoic acids (24). The pattern of WGA labeling suggests the presence of large-scale order in mature peptidoglycan, implying a complex peptidoglycan organization.

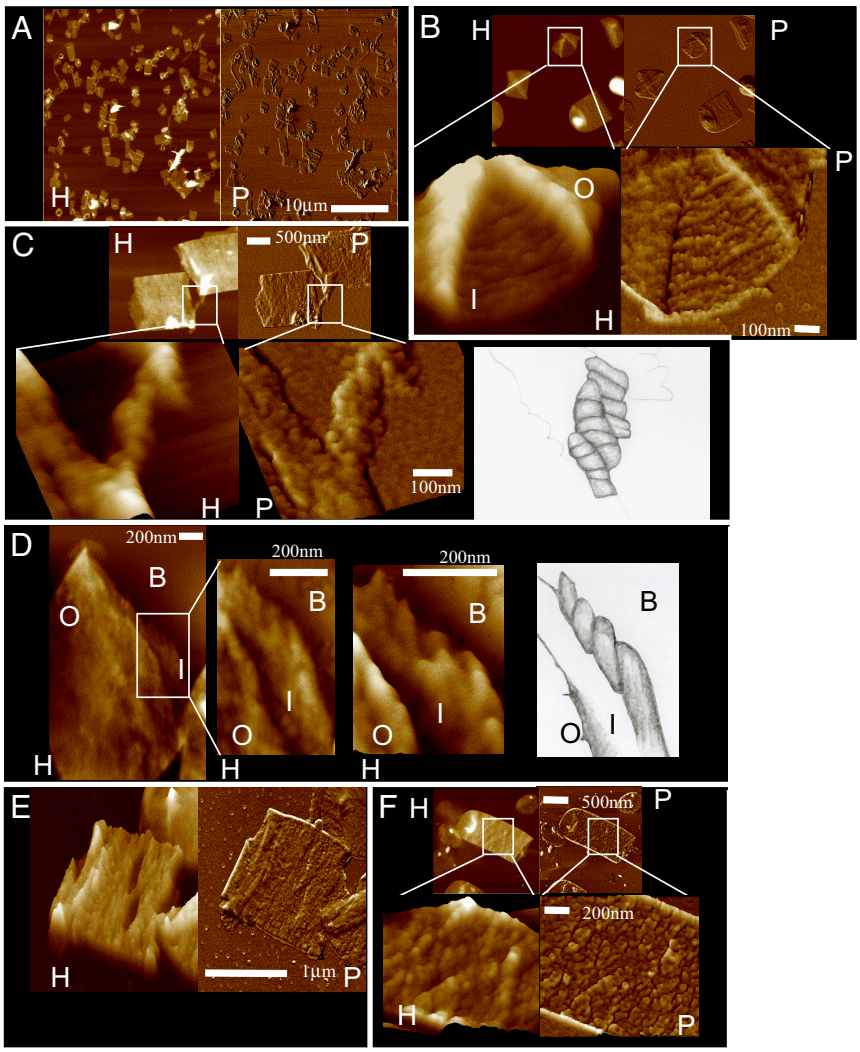

Fig. 2. *B. subtilis* sacculi architectural features revealed by AFM. (*A*) Multiple broken sacculi of *B. subtilis* showing transverse breakage plane. (*B–E*) Images of isolated, purified sacculi from gently broken cells. Images shown are top views, unless stated. (*B*) Outer (O) and inner (I) surface architecture of the cell cylinder, demonstrating an inner cabling pattern. Enlarged images have a pitch of 45° (height) and 75° (phase). (*C*) Two cylinder fragments joined by a twisted cable. Enlarged images have a pitch of 70° (height) and 80° (phase). An interpretative diagram is shown. (*D*) High-resolution image of cylinder inner surface (I). An apparent twisted cable is visible along the torn edge of the inner surface. Background (B) is labeled in these images for clarity. (Scale bars, 200 nm.) The far-right image shows a zoomed in three dimensional height image with a pitch of 60°. An interpretative diagram is shown. (*E*) View of the outer surface of the cylinder, showing a rip along a cable interface. Height image has a pitch of 70°. (*F*) Partial Atl amidase digestion (250 μg ml^{-1} Atl, 2 min at 37°C) of broken sacculi brings into relief cabling detail at the outer wall surface. Enlarged images have a pitch of 70°. In all images, height (H) and phase (P) images are shown with relevant scale bars. White boxes show area of zoom.

Our findings have important implications for cell wall architecture. Glycan strands of up to 5 μm in length preclude the proposed "scaffold" model, where glycan is orientated perpendicular to the cell membrane (10), at least for *B. subtilis*.

Analysis of Peptidoglycan Architecture. To determine how the long glycan strands fit into the peptidoglycan architecture, isolated and purified peptidoglycan sacculi of *B. subtilis* were visualized by AFM. When imaged in air, these sacculi retained the overall length and width of the intact cell with an average single wall thickness of 9 ± 1 nm (n = 22). AFM also revealed the outer surface of the sacculi to be rough, with little indication of structural features (data not shown). However, it is well known that the surface layers of peptidoglycan are hydrolyzed by endogenous autolysins that are responsible for cell wall turnover (23). Thus potentially, the outer surface of the cell wall has lost relevant architectural features because it is in the process of being dismantled and shed.

To examine the inner surface of the peptidoglycan, material was purified from cells gently broken (to retain orientating features) by a french press and visualized by AFM (Fig. 2). Cells almost always fracture basically across their short axis, suggesting an architectural feature in this plane (Fig. 2*A*), which is also conserved in *E. coli* (25). Such an orientated fracture plane argues against the "scaffold" model of peptidoglycan architecture (10), where one would not be expected. By using AFM (Fig. 2*B*), the outside of the cell wall appears rough, but where the inner surface has been revealed, "cables" of material ≈50 nm in width (average 53 ± 12 nm, n = 91) are visible running almost parallel to the short axis of the cell (average pitch of 12 ± 6°, n = 43 relative to short axis). Broken cells also showed some "unraveling" of the cables, with the extensional forces during sample preparation likely breaking the weaker bonds between cables. The "unraveling" also suggests a helical cabling arrangement (Fig. 2*C*). Cross-cabling striations can be observed with a periodicity of 25 ± 9 nm (n = 96) (Fig. 2*C*). High-resolution

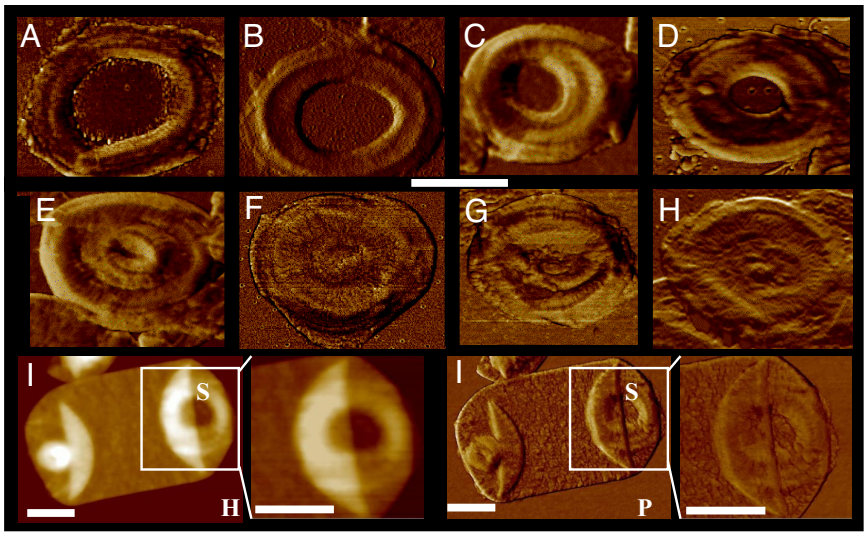

Fig. 3. AFM analysis of *B. subtilis* septal architecture. Images demonstrate architectural features during septum formation (*A–H*). Images show the progression from early septa (*A*) through to complete septa (*H*). Visible are the large cables present in several images and cross-striations traversing the larger cables. All images are phase (P) (top view). See Fig. S6 for the corresponding height images. (Scale bar, 500 nm.) (*I*) Height (H) and phase (P) images of a partially completed septum still attached to the cell. A hole in the incomplete septum (S) can be seen. The cell pole at the other end of the sacculus has a small annular feature as observed in complete septa. (Scale bars, 500 nm.)

AFM, with a resolution of 1–5 nm, revealed an apparent helical arrangement of the cross striations (Fig. 2*D*) but no finer details. Even though the outside of the cell wall has lost much of the visible cabling architecture, it still retains some features. "Rips" during breakage occur approximately across the short axis, even in material not totally fragmented (Fig. 2*E*), and partial hydrolysis with Atl amidase reveals cabling remnants in the same orientation as those observed on the inner surface (Fig. 2*F*). A gallery of supporting images is shown in Fig. S5. Studies have found 50 nm bundles of peptidoglycan fibers during protoplast regeneration in *Bacillus licheniformis* (26) and apparent striations on the cell walls of *B. subtilis* and *Lactobacillus helveticus* (27, 28).

Peptidoglycan in *B. subtilis* is biosynthesized by two sets of machinery; one dedicated primarily to the cylinder to allow cell elongation and the other to the septum for cell division (29). Our cell wall preparations contained well defined septa at all stages of formation (Fig. 3 and Fig. S6). Isolated septa have a thickened 31 ± 12 nm ($n = 10$) ridge at their cylinder junction. Within this, the septa contain apparent cabling of average 135 ± 40 nm ($n = 23$) width forming a likely spiral toward the center. Completed septa have up to three cables across their radius. Also present are striations with an average periodicity of 33 ± 19 nm ($n = 121$) running across each cable. Thus, both the cell wall cylinder and septal peptidoglycan maintain conserved architectural features, although the cable widths within the septa are generally larger.

Analysis of the Peptidoglycan Architecture of an *mreC* Mutant. AFM clearly reveals a complicated and highly organized peptidoglycan architecture with underlying features that likely relate to its function and are determined primarily during synthesis. The cell cylinder cabling architecture probably occurs as a result of the localization of the peptidoglycan biosynthetic machinery. MreC is an important part of the cytoskeletal-associated complex, arranged helically in the cell membrane (with a similar pitch to our observed "cables") and is required for the production of peptidoglycan along the cylinder (16). Importantly, a mutation in *mreC* can be stably maintained resulting in round cells, unable to make cylinder peptidoglycan and dependent on high Mg^{2+} concentrations for growth (16). Analysis of the glycan strands of the *mreC* mutant found them to vary according to growth media, being shorter than *B. subtilis* WT (Fig. 4*A*). When grown in $MgCl_2$, sucrose, and maleic acid medium (16), the WT has 8-fold more glycan material eluting before 15 min than *mreC*. However, glycan strands of *mreC* are still substantially longer than *S. aureus*, as supported by the differential labeling of *mreC* peptidoglycan by GSII and WGA (Fig. 4*B*; compared with Fig. 1*E*). Using AFM, we show that *mreC* cell walls lack the fracture plane of the WT and well defined septa. There is no evidence of regular cabling; the wall having no apparent features to differentiate the inside and outside (Fig. 4*C*). Thus, MreC, as part of the cylinder elongation biosynthetic apparatus, is required for the longest glycan strands and cabling architecture.

Conclusions

Peptidoglycan strands have a natural right-handed twist (15, 30), nascent (17) and whole material (Fig. 2 *C* and *D*) is arranged helically, and cells of *B. subtilis* can grow helically under some conditions (18). A model of peptidoglycan architecture has suggested a basic helical structure (9, 19). To explain our data, we propose that during biosynthesis, small numbers of glycan strands are polymerized and cross-linked to form a peptidoglycan "rope". This rope is then coiled into a helix with a width of ≈50 nm to form the inner surface cable structures (Fig. 5). The nascent helix (cable) is inserted into the cell wall by cross-links between two existing cables and the overlying cable interface cleaved by autolysins known to be essential for cell growth (31). The turgor pressure of the cell causes the nascent cable helix, made up of the peptidoglycan ropes, to flatten (Fig. 5), resulting in the characteristic 25 nm cross striations within the ≈50-nm cables. As part of cable maturation, the structure may become stabilized by inter/intra glycan strand cross-links. Helical features are brought into relief during Atl hydrolysis and high-resolution imaging (Fig. 2). This architecture would also accommodate very long glycan strands. The shorter glycan strands may be structurally important in the septum as specific cabling features or as a result of surface associated hydrolysis. The model predicts that the cell wall is likely only one intact cable thick with partially hydrolyzed cables also present externally.

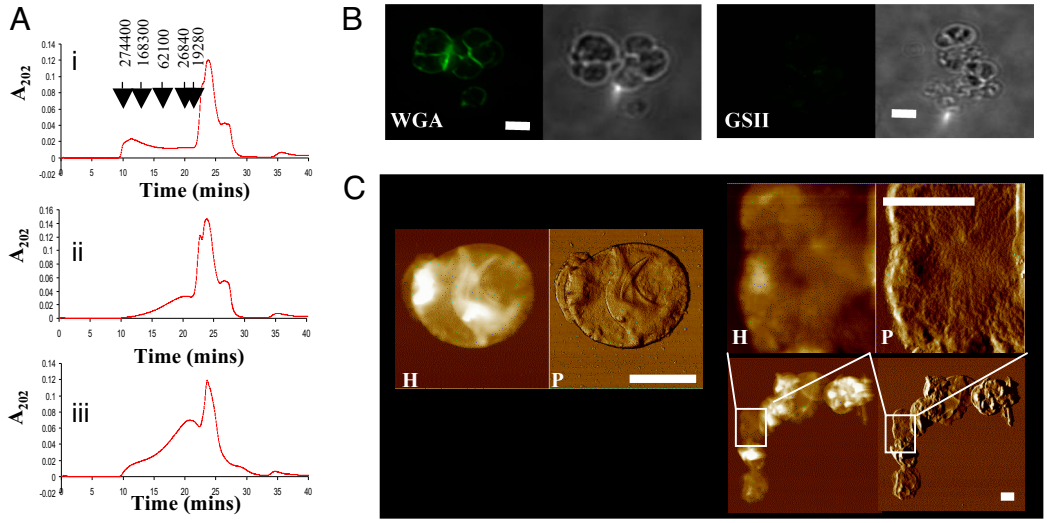

Fig. 4. Cell wall architecture of *B. subtilis mreC*. (*A*) *B. subtilis mreC* glycan strand length determination. Size exclusion chromatography of Atl amidase digested and ion exchange purified *B. subtilis* glycan material. (*i*) *B. subtilis* HR grown in MSM media. (*ii*) *B. subtilis mreC* grown in MSM media. (*iii*) *B. subtilis mreC* grown in media containing high magnesium. In (*i*), arrows indicate the elution times of linear molecular standards of polyethylene oxide (Polymer Laboratories) of masses shown. (*B*) *B. subtilis mreC* cell walls were labeled with WGA or GSII (Scale bars, 1 μm.) (*C*) AFM of *B. subtilis mreC* broken sacculi. Height (H) and phase (P) images are shown. White box shows area of zoom, revealing lack of an ordered architecture. (Scale bars, 1 μm.)

An explanation for the use of the helical cabling architecture may lie in the stress imparted on the wall by the internal osmotic pressure. In a cylindrical pressure vessel (such as *B. subtilis* rods), the circumferential stress is twice the longitudinal (32, 33). Thus, the cables provide strengthening to prevent longitudinal splitting, as supported by the fracture plane occurring approximately across the short axis during cell breakage. The recently described "periplasm" in Gram-positive bacteria with a "granular" layer provides the space to synthesize and add the cabling to the inner surface of the cell wall by using a biosynthetic machinery with enzymes protruding some distance from the cell membrane (34–36). The septum has the same basic peptidoglycan architectural features with perhaps two sets of biosynthetic machinery, one for each new pole after separation, producing a spiral septum.

This study has revealed complicated peptidoglycan architecture in *B. subtilis*. A mutant lacking the organization cannot survive under normal conditions, suggesting strict functional constraints on architecture. How peptidoglycan is able to maintain cell shape and viability is currently unknown. However, our analysis provides the experimental framework to test one of the most basic facets of growth and division in *B. subtilis* and more widely across bacteria.

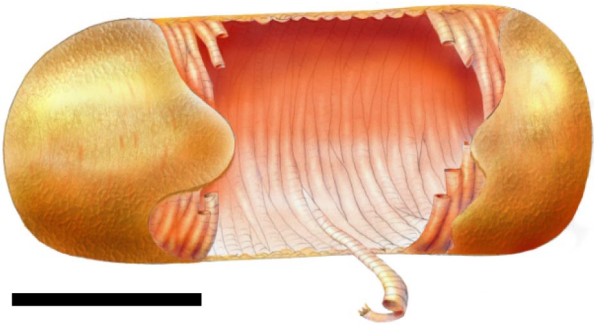

Fig. 5. Model of *B. subtilis* cell wall peptidoglycan architecture. Image is of a cell wall cylinder peptidoglycan architecture showing cable orientation with coiled substructure. Both cables and cross striations are shown. (Scale bar, 1 μm.)

Materials and Methods

Size Exclusion Chromatography of *B. subtilis* Glycan Strands. *B. subtilis* peptidoglycan was purified as described (4) and digested overnight with the recombinant amidase domain of Atl (see *SI Text*) (37). Glycan was purified from the resulting soluble material by using a MonoS ion exchange chromatography column, as described (see *SI Text*) (6), concentrated three times by using SpeedVac, and applied to a $TSKgelSW_{4000}$ size exclusion HPLC column (Tosoh). Elution was in 100 mM sodium phosphate buffer, pH 2 at 0.5 ml min^{-1}. To confirm the material as glycan, it was digested overnight with the muramidase Cellosyl and reapplied to the column. To radiolabel peptidoglycan, cells were grown in minimal media containing *N*-acetyl [^{14}C]glucosamine (38). Details of the methods and additional controls can be found in *SI Text*.

Measurement of Glycan Strands by Using AFM. High-mass glycan from the size exclusion column (eluted at 10–12.5 min) was collected and desalted by using a 10,000 MW cut-off filter (Amersham). The pH was adjusted to 7, and the sample was equilibrated overnight at 4°C. A 1:8 dilution of the sample was applied to a cleaned coverslip and N_2 dried. AFM images were collected in air by using a Veeco D3100 microscope, operated in Tapping Mode™, with Olympus silicon cantilevers and a nominal spring constant 50 Nm^{-1}.

WGA and GSII Lectin Labeling. Exponential phase cells were harvested, bathed in 5% wt/vol SDS at 50°C for 30 min, washed, and resuspended in 48% vol/vol hydrofluoric acid overnight. Cells were then washed, resuspended in 250 μl water, and then incubated with 40 μM WGA or GSII (with 1 mM $CaCl_2$) for 30 min. Cells were then washed to remove excess lectin, resuspended in 50 mM glucose at an appropriate dilution, and mounted on a poly-L-lysine coated slide. Images were collected by using a Deltavision microscope (Applied Precision) and deconvolved by using Softworx version 3.5.1.

AFM of *B. subtilis* Sacculi. Exponential phase cells were harvested, boiled (7 min), and broken by using a french press at a pressure of 500 psi. Peptidoglycan was then purified as described (4). For optimal imaging, sacculi were diluted in MilliQ water, applied to a coverslip or to mica, and air dried before AFM imaging as for glycan strands.

ACKNOWLEDGMENTS. We thank M. Williamson, P. Artymiuk, and M. Buttner for critical discussions and reading of the manuscript, R. Adams for help with Fig. 5, J. Garcia-Lara for help using the Deltavision microscope, J. Errington and M. Leaver (both University of Newcastle, Newcastle upon Tyne, U.K.) for providing strains, and H. Crossley for technical support. This work was supported by the Biotechnology and Biological Sciences Research Council, the Engineering and Physical Sciences Research Council, and Wellcome Trust Grant GR077544AIA for the light microscopy facility.

1. Archibald AR, Hancock IC, Harwood CR (1993) *Bacillus subtilis and other Gram-positive bacteria*, eds Sonenshein AL, Hoch JA, Losick R (American Society for Microbiology, Washington DC), pp 381–410.
2. Foster SJ, Popham DL (2002). *Bacillus subtilis and Its Closest Relatives: From genes to cells*, eds Sonenshein AL, Hoch JA, Losick R (American Society for Microbiology, Washington DC), pp 21–41.
3. Glauner B (1988) Separation and quantification of muropeptides with high-performance liquid chromatography. *Anal Biochem* 172:451–464.
4. Atrih A, Bacher G, Allmaier G, Williamson MP, Foster SJ (1999) Analysis of peptidoglycan structure from vegetative cells of *Bacillus subtilis 168* and role of PBP 5 in peptidoglycan maturation. *J Bacteriol* 181:3956–3966.
5. Harz H, Burgdorf K, Holtje JV (1990) Isolation and separation of the glycan strands from murein of *Escherichia coli* by reversed-phase high-performance liquid chromatography. *Anal Biochem* 190:120–128.
6. Boneca IG, Huang ZH, Gage DA, Tomasz A (2000) Characterization of *Staphylococcus aureus* cell wall glycan strands, evidence for a new beta-N-acetylglucosaminidase activity. *J Biol Chem* 275:9910–9918.
7. Ward JB (1973) The chain length of the glycans in bacterial cell walls. *Biochem J* 133:395–398.
8. Koch AL (1998) Orientation of the peptidoglycan chains in the sacculus of *Escherichia coli*. *Res Microbiol* 149:689–701.
9. Verwer RH, Nanninga N, Keck W, Schwarz U (1978) Arrangement of glycan chains in the sacculus of *Escherichia coli*. *J Bacteriol* 136:723–729.
10. Dmitriev BA, *et al.* (2003) Tertiary structure of bacterial murein: The scaffold model. *J Bacteriol* 185:3458–3468.
11. Dmitriev BA, Toukach FV, Holst O, Rietschel ET, Ehlers S (2004) Tertiary structure of *Staphylococcus aureus* cell wall murein. *J Bacteriol* 186:7141–7148.
12. Vollmer W, Holtje JV (2004) The architecture of the murein (peptidoglycan) in gram-negative bacteria: Vertical scaffold or horizontal layer(s)? *J Bacteriol* 186:5978–5987.
13. Touhami A, Jericho MH, Beveridge TJ (2004) Atomic force microscopy of cell growth and division in *Staphylococcus aureus*. *J Bacteriol* 186:3286–3295.
14. Plomp M, Leighton TJ, Wheeler KE, Hill HD, Malkin AJ (2007) *In vitro* high-resolution structural dynamics of single germinating bacterial spores. *Proc Natl Acad Sci USA* 104:9644–9649.
15. Meroueh SO, *et al.* (2006) Three-dimensional structure of the bacterial cell wall peptidoglycan. *Proc Natl Acad Sci USA* 103:4404–4409.
16. Leaver M, Errington J (2005) Roles for MreC and MreD proteins in helical growth of the cylindrical cell wall in *Bacillus subtilis*. *Mol Microbiol* 57:1196–1209.
17. Daniel RA, Errington J (2003) Control of cell morphogenesis in bacteria: Two distinct ways to make a rod-shaped cell. *Cell* 113:767–776.
18. Tilby MJ (1977) Helical shape and wall synthesis in a bacterium. *Nature* 266:450–452.
19. Mendelson NH (1976) Helical growth of *Bacillus subtilis*: A new model of cell growth. *Proc Natl Acad Sci USA* 73:1740–1744.
20. Braun V (1973) Molecular organization of the rigid layer and the cell wall of *Escherichia coli*. *J Infect Dis* 128:9–16.
21. Sizemore RK, Caldwell JJ, Kendrick AS (1990) Alternate gram staining technique using a fluorescent lectin. *Appl Environ Microbiol* 56:2245–2247.
22. Lyer PN, Wilkinson KD, Goldstein LJ (1976) An N-acetyl-D-Glycosamine binding lectin from *Bandeiraea simplicifolia* seeds. *Arch Biochem Biophys* 177:330–333.
23. Smith TJ, Blackman SA, Foster SJ (2000) Autolysins of *Bacillus subtilis*: Multiple enzymes with multiple functions. *Microbiol* 146:249–262.
24. Henriques AO, Glaser P, Piggot PJ, Moran CP, Jr (1998) Control of cell shape and elongation by the *rodA* gene in *Bacillus subtilis*. *Mol Microbiol* 28:235–247.
25. Verwer RWH, Beachey EH, Keck W, Stoub AM, Poldermans JE (1980) Orientated fragmentation of *Escherichia coli sacculi* by sonication. *J Bacteriol* 141:327–332.
26. Elliott TSJ, Ward JB, Wyrick PB, Rogers HJ (1975) Ultrastructural study of the reversion of protoplasts of *Bacillus lichenformis* to *Bacilli*. *J Bacteriol* 124:905–917.
27. Verwer RWH, Nanninga N (1976) Electron microscopy of isolated cell walls of *Bacillus subtilis var niger*. *Arch Microbiol* 109:195–197.
28. Firtel M, Henderson G, Sokolov I (2004) Nanosurgery: Observation of peptidoglycan strands in *Lactobacillus helveticus* cell walls. *Ultramicroscopy* 101:105–109.
29. Lleo MM, Canepari P, Satta G (1990) Bacterial cell shape regulation: Testing of additional predictions unique to the two-competing-sites model for peptidoglycan assembly and isolation of conditional rod-shaped mutants from some wild-type cocci. *J Bacteriol* 172:3758–3771.
30. Leps B, Labischinski H, Bradaczek H (1987) Conformational behaviour of the polysaccharide backbone of the murein. *Biopolymers* 26:1391–1406.
31. Bisicchia P, *et al.* (2007) The essential YycFG two-component system controls cell wall metabolism in *Bacillus subtilis*. *Mol Microbiol* 65:180–200.
32. Gordon JE (1978) *Structures: Or Why Things Don't Fall Down* (Da Capo Press, New York), pp 113–131.
33. Koch AL (1995) *Bacterial growth and form* (Chapman and Hall, New York), pp 143–172.
34. Matias VR, Beveridge TJ (2005) Cryo-electron microscopy reveals native polymeric cell wall structure in *Bacillus subtilis 168* and the existence of a periplasmic space. *Mol Microbiol* 56:240–251.
35. Zuber B, *et al.* (2006) Granular layer in the periplasmic space of gram-positive bacteria and fine structures of *Enterococcus gallinarum* and *Streptococcus gordonii* septa revealed by cryo-electron microscopy of vitreous sections. *J Bacteriol* 188:6652–6660.
36. Lim D, Strynadka NCJ (2002) Structural basis for the β-lactam resistance of PBP2a from methicillin-resistant *Staphylococcus aureus*. *Nat Struct Biol* 9:870–876.
37. Clarke SR, *et al.* (2006) Identification of *in vivo*-expressed antigens of *Staphylococcus aureus* and their use in vaccinations for protection against nasal carriage. *J Infect Dis* 193:1098–1108.
38. Pooley HM (1976) Turnover and spreading of old wall during surface growth of. *Bacillus subtilis* during growth in different media. *J Bacteriol* 125:1127–1138.